

Evaluation of the liver targeting and anti-liver cancer activity of artesunate-loaded and glycyrrhetic acid-coated nanoparticles

XU-WANG PAN¹, JIN-SONG HUANG², SHOU-RONG LIU², YI-DAN SHAO¹, JIAN-JUN XI¹,
RUO-YU HE¹, TING-TING SHI¹, RANG-XIAO ZHUANG¹ and JIAN-FENG BAO²

Departments of ¹Pharmaceutical Preparation and ²Liver Disease,
Hangzhou Xixi Hospital, Hangzhou, Zhejiang 310023, P.R. China

Received April 11, 2023; Accepted August 24, 2023

DOI: 10.3892/etm.2023.12215

Abstract. Globally, liver cancer ranks among the most lethal cancers, with chemotherapy being one of its primary treatments. However, poor selectivity, systemic toxicity, a narrow treatment window, low response rate and multi-drug resistance limit its clinical application. Liver-targeted nanoparticles (NPs) exhibit excellent targeted delivery ability and promising effectivity in treating liver cancer. The present study aimed to investigate the liver-targeting and anti-liver cancer effect of artesunate (ART)-loaded and glycyrrhetic acid (GA)-decorated polyethylene glycol (PEG)-poly(lactic-co-glycolic acid) (PLGA) (ART/GA-PEG-PLGA) NPs. GA-coated NPs significantly increased hepatoma-targeted cellular uptake, with micropinocytosis and caveolae-mediated endocytosis as its chief internalization pathways. Moreover, ART/GA-PEG-PLGA NPs exhibited pro-apoptotic effects on HepG2 cells, mainly via the induction of a high level of reactive oxygen species, decline in mitochondrial membrane potential and induction of cell cycle arrest. Additionally, ART/GA-PEG-PLGA NPs induced internal apoptosis pathways by upregulating the activity of cleaved caspase-3/7 and expression of cleaved poly (ADP-Ribose)-polymerase and Phos-p38 mitogen-activated protein kinase in HepG2 cells. Furthermore, ART/GA-PEG-PLGA NPs exhibited higher liver accumulation and longer mean retention time, resulting in increased bioavailability. Finally, ART/GA-PEG-PLGA NPs promoted the liver-targeting distribution of ART, increased the retention time and promoted its antitumour effects *in vivo*.

Therefore, ART/GA-PEG-PLGA NPs afforded excellent hepatoma-targeted delivery and anti-liver cancer efficacy, and thus, they may be a promising strategy for treating liver cancer.

Introduction

Liver cancer is one of the deadliest types of cancer globally (1) and is ranked fourth and second regarding incidence and mortality in China (2). Hepatitis B and C viral infection, alcohol consumption and non-alcoholic fatty liver disease are the risk factors of liver cancer (3). Although surgical resection remains the most effective treatment for liver cancer, only patients with unilobar tumours with preserved liver function and without hepatic vascular invasion metastases qualify for surgery. However, surgical resection alone cannot eradicate the tumour completely (4). Currently, chemotherapy remains an important adjuvant therapy for liver cancer. Nevertheless, its clinical use is often seriously restricted owing to poor selectivity and adverse reactions (5). In addition, despite the rapid progress in molecular-targeted therapies and immunotherapy triggered by the emergence of small-molecule targeted drugs, obstacles such as a narrow treatment window, low response rate and multidrug resistance seriously hinder the clinical application of these agents (6,7). Globally, although the morbidity and mortality of liver cancer are increasing, the improvement and efficacy of its major treatments remain seriously limited. Thus, there is a pressing need to formulate novel curative protocols for liver cancer that are safer and more effective.

Over the past two decades, nano-targeted delivery systems have shown promise for tumour treatment (8,9). Nano-targeted drug-delivery systems (DDSs) can not only passively target the tumour by enhancing the penetration and retention (EPR) effect (10,11) but also actively target tumour blood vessels and cells via the targeted modification of carrier materials to promote drug accumulation in tumours, improve drug safety and reduce adverse events incidence (12-14). Moreover, using a nano-targeted delivery system, chemotherapeutic drugs can be made more soluble and stable and their affinity toward blood proteins can be reduced (15,16). More importantly, polymer-based nanoparticles (NPs) exhibit high biocompatibility, biodegradability and structural generality, thereby serving as additional alternatives to custom-made drug-delivery vehicles according to specific requirements with

Correspondence to: Professor Rang-Xiao Zhuang, Department of Pharmaceutical Preparation, Hangzhou Xixi Hospital, 2 Hengbu Road, Hangzhou, Zhejiang 310023, P.R. China
E-mail: 421867177@qq.com

Professor Jian-Feng Bao, Department of Liver Disease, Hangzhou Xixi Hospital, 2 Hengbu Road, Hangzhou, Zhejiang 310023, P.R. China
E-mail: zbjf1972@aliyun.com

Key words: glycyrrhetic acid, artesunate, targeted delivery, liver cancer, antitumor effect

excellent treatment efficacy and safety performance (17-19). In addition, NP systems can be administered orally, locally, via injection, systemically and through the lungs, according to the specific demands (20-22). Numerous nano-systems have afforded improved therapeutic results in animal models, with some of them entering clinical trials and some even being translated to clinical practice (23-26). However, complete translation of success *in vivo* experiments into clinical use remains challenging. Therefore, previously, 'variable-size' and 'stimulus-response' strategies, such as the core-shell strategy, surface carrying tactic and Trojan horse tactic have been proposed (27-29). The use of new functional carrier materials or targeted chemical modifications has become a breakthrough in designing new drug-delivery systems.

Targeted drug delivery can occur in two forms: A passive targeting pattern, which is based on an enhanced EPR action; and an active targeting pattern, which depends on the introduction of targeting ligands into the NPs, for drug distribution to a specific site (30). The combination of the two patterns into one NP can significantly improve the selective accumulation effectiveness of the targeted drug-delivery system and enhance its medication delivery. Regarding active targeting, NP surfaces can be coated with certain specific parts aimed at specific receptors that are overexpressed in the tumour microenvironment or on the exterior of cancerous tissues (31).

Glycyrrhetic acid (GA) is mostly obtained from the underground part of *Glycyrrhiza glabra* L. Negishi *et al* (32) first reported that rat hepatocyte membranes contained a GA-binding site, which was later demonstrated to be the protein kinase C α , which is highly expressed in liver tumour cells at a level that is 1.5- to 5-fold higher than that in normal hepatocytes (33,34). Owing to the specific recognition ability of GA receptors and their protective effects on normal liver tissues, GA-modified drugs and NPs exhibit considerable liver-targeting ability and targeted induction of apoptosis in liver cancer cells and have been used to manage liver-related diseases in numerous countries and regions (35-39).

Artesunate (ART) is an artemisinin derivative that has been a focus of antitumour drug research and has shown favorable inhibitory effects on liver cancer (40,41). However, the low solubility, easy degradation in water, short half-life, poor selectivity for tumours and low bioavailability of ART significantly limits its antitumour effects and subsequent clinical applications (42,43). Thus, the incorporation of ART into novel nano-preparations is proposed. GA-coated and ART-loaded polyethylene glycol (PEG)-poly (lactic-co-glycolic acid) (PLGA) (ART/GA-PEG-PLGA) NPs were previously prepared (42). In the present study, the cellular uptake of these NPs mediated by the GA receptor as well as their intracellular mechanisms, pro-apoptotic effects, potential mechanisms, pharmacokinetics, biological distribution and antitumour effects, were examined. Thus, the collective results of the present study may provide insights into the development of a drug-delivery system for effective liver cancer treatment.

Materials and methods

Materials. Eagle's Minimal Essential Medium (EMEM) and F-12K were purchased from Gibco; Thermo Fisher Scientific, Inc.; pargenzyme was also procured from Gibco;

Thermo Fisher Scientific, Inc.; 3,3'-dioctadecyloxycarbocyanine perchlorate (DiO) was purchased from Beyotime Institute of Biotechnology. Chlorpromazine, wortmannin, genistein and methyl- β -cyclodextrin were obtained from Selleck Chemicals. Reactive oxygen species (ROS, cat. no. S0033M), JC-1 (cat. no. C2005) and cell apoptosis and cell cycle detection kits (cat. no. C1052) were purchased from Beyotime Institute of Biotechnology. The Annexin V-FITC/PI double staining apoptosis detection kit (cat. no. KGA-108) was obtained from Nanjing KeyGen Biotech Co., Ltd.; marker10-180 (BE2666-250) was procured from EASYBIO. Ponceaux (cat. no. A100860) and phenylmethanesulfonyl fluoride (cat. no. 100754) were provided by Sangon Biotech Co., Ltd. ProBlott membrane regenerative fluid ZN1923 was purchased from Beijing Biolab Technology Co., Ltd. Anti-caspase-3 (cat. no. 9662), anti-caspase-7 (cat. no. 9492), anti-poly-(ADP-ribose)-polymerase (PARP) (cat. no. 9542), anti-phosphorylated-p38 mitogen-activated protein kinase (MAPK) (cat. no. 9211) and anti-p38 MAPK (cat. no. 9212) antibodies were obtained from Cell Signaling Technology, Inc.

Cell culture. The HepG2 cell line (cat. no. HB-8065; cultured from liver cancer, cells with high GA receptor expression) and A549 cell line (cat. no. CCL-185; cultured from lung cancer, cells with low GA receptors expression) were purchased from the American Tissue Culture Collection (ATCC). Hep3B-luc was purchased from Wuxi Aptec Co., Ltd. The HepG2 cell line was authenticated by Procell Life Science & Technology Co., Ltd. using short tandem repeat (STR) analysis. DNA was extracted from the HepG2 cells using Chelex100 (cat. no. 1432832; Bio-Rad Laboratories, Inc.). The 20 STRs, including the Amelogenin locus, were amplified using the 21 CELLID system and separated using ABI 3130X1 Genetic Analyzer (Thermo Fisher Scientific, Inc.). The signals were subsequently analysed using GeneMapper IDX software (v1.6; Applied Biosystems) and compared via the ATCC, DSMZ (<https://www.dsmz.de/>), JCRB (<https://cellbank.nibiohn.go.jp/>) and Cellosaurus (<https://www.cellosaurus.org/>) databases. The authentication results revealed that the DNA of the cell line matched perfectly with the type of cell lines in a cell line retrieval.

Animal studies. Female BALB/c nude mice (total number, 24; age, 6-8 weeks; weight, 18-22 g) were obtained from Zhejiang Vitonolihua Experimental Animal Technology Co., Ltd. Male Sprague Dawley (SD) rats (total number, 8; age, 6-8 weeks; weight, 244-254 g) were obtained from Jihui Laboratory Animal Co. Ltd. All mice and rats were kept in specific pathogen-free (SPF) environment with a temperature and humidity of 20-26°C and 40-70%, respectively, under a 12-h light/dark cycle. All mice were provided water and food *ad libitum*. The rats were fasted overnight and fed 4 h after dose administration, while they had free access to water. All animal tests were performed according to the National Research Council's Guide for the Care and Use of Laboratory Animals.

Uptake of NPs into HepG2 cells and their intracellular localization. NPs were prepared and characterized as previously reported (42). The uptake of NPs into HepG2 cells and their intracellular mechanisms were investigated.

Cellular uptake determination. To estimate the hepatoma-targeting ability of GA-coated NPs, the affinity of NPs toward HepG2 and A549 cells was compared. The fluorescent probe Nile red (NR) was loaded onto the GA-modified NP to trace its uptake. Control groups were generated using normal cells, free-NR and NR-encapsulated unmodified NPs (NR/PEG-PLGA). The cells were seeded into each well at a density of 2×10^5 cells. Following an additional 24-h incubation period, the cells were co-incubated with each group of drugs at the equal NR of $50 \mu\text{g/ml}$. Subsequently, they were washed with cold phosphate-buffered solution (PBS) thrice, and then incubated for an additional 0.5, 1 or 4 h. The fluorescence intensity in cells was analysed via flow cytometry (FCM; Beckman DxFlex Flow Cytometer; with Cytexpert 2.5 software; Beckman Coulter, Inc.).

Intracellular localization. HepG2 cells were seeded at a density of 2×10^4 cells/well of microscope slides and incubated at 37°C in an atmosphere containing 5% CO_2 for 24 h. Next, they were incubated with each drug group (free-NR, NR/PEG-PLGA or NR/GA-PEG-PLGA NPs) with an equivalent NR of $50 \mu\text{g/ml}$ for 4 h. The cells were washed thrice using cold PBS and the cell membranes were stained with DiO at $10 \mu\text{M}$. Subsequently, the cells were washed thrice and fixed on ice with 4% paraformaldehyde for 15 min followed by three washes and staining with DAPI ($10 \mu\text{g/ml}$) for 5 min at room temperature. A confocal laser scanning microscope (CLSM; LSCM 780; Carl Zeiss AG) was used to acquire fluorescence images.

Uptake pathway identification. Pharmacological inhibitors were used to date the uptake pathway. The pharmacological inhibitors were used at the following concentrations: free-GA, $10 \mu\text{M}$; 2-deoxyglucose (cat. no. D8375; Sigma-Aldrich; Merck KGaA), 20 mM; chlorpromazine, $10 \mu\text{M}$; wortmannin, $10 \mu\text{M}$; genistein, $50 \mu\text{M}$; and methyl- β -cyclodextrin, 5 mM. HepG2 cells from each group were pre-incubated with their indicated inhibitors for 1 h followed by the administration of NR/GA-PEG-PLGA NPs at a NR concentration of $50 \mu\text{g/ml}$ and incubation for an additional 4 h. Subsequently, the cells were washed with cold PBS thrice and analysed using FCM.

Pro-apoptotic effects and relevant mechanisms

Determination of intracellular ROS. The oxidative conversion of 2',7'-dichlorodihydrofluorescein diacetate (DCFH-DA) to dichlorofluorescein (DCF; 488 nm excitation wavelength) is the foundation for measuring ROS emergence in cells. The HepG2 cells ($3 \times 10^5/\text{ml}$) were treated with blank NPs, free-ART, ART/PEG-PLGA or ART/GA-PEG-PLGA at an ART concentration of 5 mg/ml. After 72 h of culture at 37°C with 5% CO_2 , the cells were digested with trypsin without EDTA and centrifuged for 5 min at $400 \times g$ and 4°C . The cells were subsequently cultured for 20 min in the dark in medium containing $5 \mu\text{M}$ DCFH-DA at 37°C . Intracellular ROS interacts with DCFH-DA to produce green fluorescent DCF, whose strength was determined via FCM over 0.5 h.

Mitochondrial membrane potential measurement. For the quantitation assay, the HepG2 cells were seeded at a density of 1×10^5 cells/well. After 12 h of culture at 37°C with 5% CO_2 , the cells were washed with PBS and continuously cultured for 72 h

with free-ART, ART/PEG-PLGA or ART/GA-PEG-PLGA at an ART concentration of 5 mg/ml. Then, the cells were washed, collected and mixed in a JC-1 dye working solution according to the manufacturer's protocol, followed by FCM analysis.

Cell cycle distribution. The effects of ART/GA-PEG-PLGA NPs on HepG2 cell block were evaluated using FCM. The cells were treated with free-ART, ART/PEG-PLGA or ART/GA-PEG-PLGA at an ART concentration of 5 mg/ml for 72 h, then collected and fixed in 70% ethanol overnight at 4°C . Next, the HepG2 cells were harvested and treated with RNase at $50 \mu\text{g/ml}$ at 37°C for 0.5 h followed by incubation with propidium iodide (PI) at $65 \mu\text{g/ml}$ in an ice bath for 0.5 h in the dark and analysis using FCM.

Annexin V-FITC/PI double staining. Necrosis and apoptosis in the ART/GA-PEG-PLGA NP-treated HepG2 cells were determined using Annexin V-FITC. The cells were seeded at a density of 6×10^5 cells/well and treated with free-ART, ART/PEG-PLGA or ART/GA-PEG-PLGA at an equal ART concentration of 5 mg/ml for 72 h. The cells were subsequently collected, re-suspended in $500 \mu\text{l}$ binding buffer, dyed with $5 \mu\text{l}$ Annexin V-FITC and $5 \mu\text{l}$ PI solution at room temperature in the dark for 15 min and finally assessed using FCM.

Western blot analyses. The mechanisms underlying the apoptosis induced by the different ART preparations were investigated via western blotting. The HepG2 cells were treated with free-ART, ART/PEG-PLGA or ART/GA-PEG-PLGA at an ART concentration of 5 mg/ml for 72 h. The total proteins were extracted via a radio-immuno-precipitation assay lysis buffer (Beyotime Institute of Biotechnology) and concentration was measured using a BCA protein assay kit (Abcam). The extract was separated by 10% SDS-PAGE; sample size, $60 \mu\text{g}$ and then transferred onto a polyvinylidene fluoride (PVDF) membrane (Merck KGaA). Following blocking with 5% BSA for 60 min at room temperature, the membrane was incubated with a specific primary antibody (dilution ratio, 1:1,000) overnight at 4°C . The PVDF membrane was subsequently washed thrice with TBST (0.1% Tween-20, 10 min each time) and incubated with the corresponding secondary antibody [goat anti-rabbit IgG H&L (HRP) and rabbit anti-mouse IgG H&L (HRP); cat. no. ab6721 and ab6728, respectively; 1:10,000 dilution; Abcam] at room temperature for 1 h. Protein bands were revealed using an ECL luminescent reagent (cat. no. 32209; Thermo Fisher Scientific, Inc.). The density of the bands was quantified using Image-Pro Plus 6.0 (Tanon, Science and Technology Co., Ltd.).

Pharmacokinetics studies. Male SD rats were randomized into two groups (i.e., free-ART and ART/GA-PEG-PLGA NPs). Free-ART was dissolved in a 0.5% carboxymethylcellulose sodium (CMC-Na) solution (v/v). The two formulations were administered intragastrically at an ART dose of 50 mg/kg. At the indicated time points (5 and 15 min; and 0.5, 1, 2, 4, 8, 12, 24 and 48 h), blood samples were collected and separated to obtain the plasma. ART was detected using liquid chromatography-mass-mass-22 (LC/MS/MS-22) spectrometry analysis [Triple Quad 6500; Shanghai AB SCIEX Analytical Instrument Trading Co; ionisation mode used: Negative. Parent (m/z)/daughter (m/z): Artesunate-Q1/Q3

masses, 407.20/261.00 Da; dihydroartemisinin-Q1/Q3 masses, 307.30/261.10 Da; Glipizide-Q1/Q3 masses, 446.20/321.10 Da. Flow rate, 0.40 ml/min; column temperature, 60°C; pressure range (pump A/B), 0.0-100.0 MPa]. The Data Analysis System v3.0 (BioGuider Co.) was used to analyze the pharmacokinetics parameters. Carbon dioxide euthanasia was performed for rats: Rats were placed into the euthanasia box and carbon dioxide was flushed in and adjusted to 50% vol/min. The state of the rats was carefully observed and input was continued for 1 min after loss of consciousness. Death of rats was confirmed through cervical dislocation.

Tumour cell inoculation. A suspension of 0.02 ml Hep3B-luc tumour cells (including 3×10^6 cells; ratio of PBS to Matrigel®, 1:1) was seeded *in situ* on the left hepatic lobe of each mouse. On day 7 following the cell inoculation, the tumour bio-fluorescence signal was measured using IVIS Lumina III, and nine mice were selected based on the intensity of the fluorescence signal and body weight.

Hepatoma-targeted and bio-distribution detection. NR was used as the fluorescent probe to detect the hepatoma-targeting ability and bio-distribution of GA-PEG-PLGA NPs. The tumour model mice were randomized into three groups and administered the different NR preparations intragastrically at an NR dose of 20 mg/kg. The fluorescence signal distribution of NR was detected *in vivo* at 0.5, 2, 4 and 8 h following administration. Subsequently, the mice were euthanized, the main organs (heart, liver, spleen, lung and kidney) were harvested and the intensity of the NR signal was detected in each organ.

Antitumour activity. The antitumour activity of ART/GA-PEG-PLGA NPs was investigated in female BALB/c nude mice (age, 6-8 weeks) bearing Hep3B-luc *in situ* transplanted tumours. When the fluorescence signal intensity of the implanted tumour cells reached $\sim 10^7$, the mice were randomized into four groups (i.e., control, free-NR, NR/PEG-PLGA NPs and NR/GA-PEG-PLGA NPs) and treated intragastrically with different ART preparations at an ART concentration of 50 mg/kg once daily for 24 days, with the exception of the control group. The tumour fluorescence signal and body weight of the mice were measured twice per week. The mice were humanely euthanized when they lost >20% body weight because of weakness or near-death conditions. The inhibition rate of tumor (IRT) was calculated using the following formula: i) Based on the fluorescence signal: $IRT = [(ROI_{control} - ROI_{drug}) / ROI_{control}] \times 100\%$ (where ROI_{drug} : Mean tumour fluorescence value of the treated mice; $ROI_{control}$: Mean tumour fluorescence value of the control mice); ii) Based on the tumour weight: $IRT = [(W_{control} - W_{drug}) / W_{control}] \times 100\%$ (where W_{drug} : mean tumour weight of the treated mice; $W_{control}$: Mean tumour weight of the control mice).

The survival rates of the mice were calculated over a 24-day period. Their survival time was calculated based on the grouping day (pg-d0) and the corresponding survival curves were drawn.

The euthanasia method of mice was the same as that of rats aforementioned. Lastly, the tumours and major organs (heart, liver, spleen, lungs and kidneys) were collected at 4 h

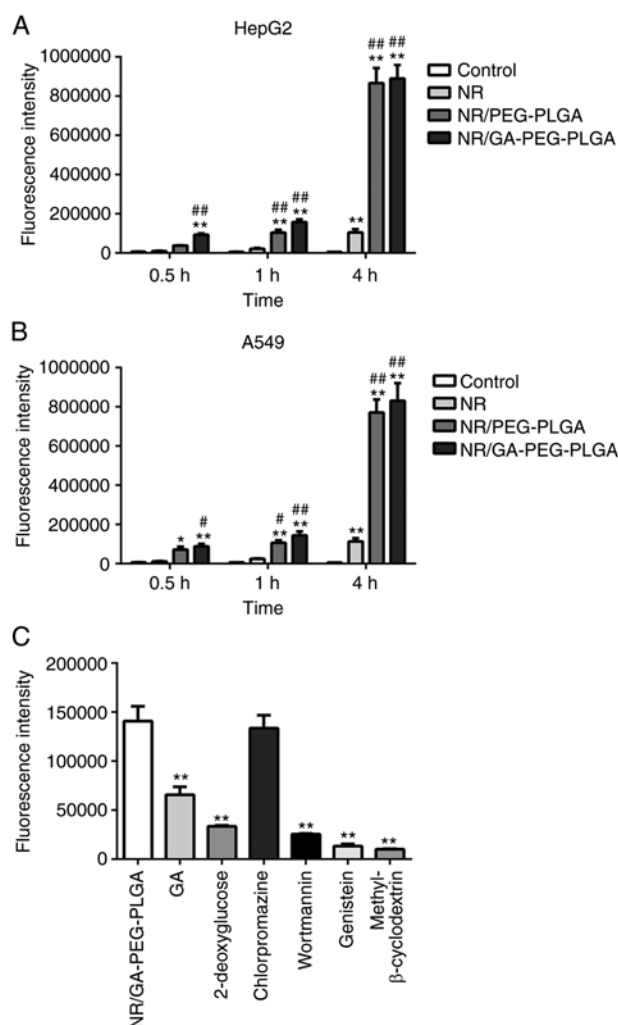


Figure 1. Immunofluorescence of (A) HepG2 and (B) A549 cells. The results are presented as the mean \pm standard deviation ($n=3$). * $P<0.05$ and ** $P<0.01$ vs. the control group; # $P<0.05$ and ## $P<0.01$ vs. the NR group. (C) Evaluation of the uptake mechanisms of NR/GA-PEG-PLGA NPs in HepG2 cells in the presence of free-GA and various endocytosis inhibitors. ** $P<0.01$ vs. the NR/GA-PEG-PLGA group. NR, Nile red; GA, glycyrrhetic acid; NPs, liver-targeted nanoparticles; PEG-PLGA, polyethylene glycol-poly (lactic-co-glycolic acid).

after the last drug administration and immersed in formalin and paraffin followed by haematoxylin and eosin staining for 5 min and 7 sec, respectively, at room temperature. The tissues were observed using light microscope (ECLIPSE E100; Nikon Corp.). The tumours were also weighted.

Statistical analysis. All data are expressed as the mean \pm standard deviation and were analysed via one-way analysis of variance followed by a Tukey's post-hoc test using SPSS (version 19; IBM Corp.). For all the results, $P<0.05$ and $P<0.01$ were considered to indicate a statistically significant and extremely significant difference, respectively.

Results

Uptake of NPs and intracellular mechanism. To identify the specific hepatoma target function of GA-coated NPs, the uptake of NR-labelled NPs into HepG2 and A549 cells, which express

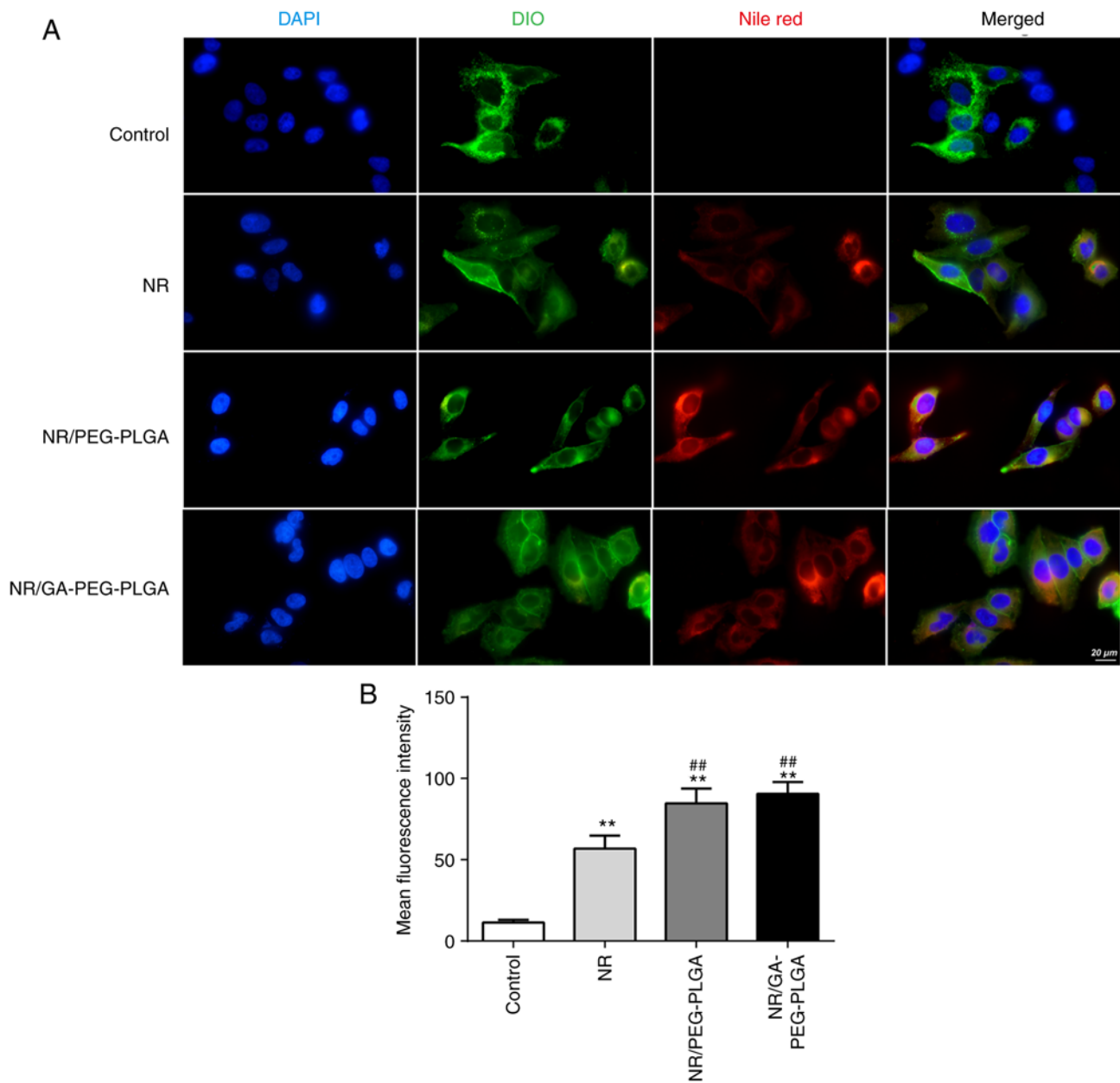


Figure 2. Immunofluorescence staining was performed to investigate the cellular internalization of NR. (A and B) Cell nuclei were stained blue using DAPI and cytoplasmic membranes were stained green using (DiO). The results are presented as the mean \pm standard deviation (n=3). **P<0.01 vs. the control group; ##P<0.01 vs. the NR group. NR, Nile red; DiO, 3,3'-diiodoacetylcarboxyanine perchlorate; GA, glycyrrhetic acid; PEG-PLGA, polyethylene glycol-poly(lactic-co-glycolic acid).

GA receptors at high and low levels, respectively, was assessed. As shown in Fig. 1A and B, the untreated cells or those incubated with free-NR exhibited little fluorescence. The HepG2 and A549 cells incubated with NR/GA-PEG-PLGA NPs or NR/PEG-PLGA NPs expressed significantly higher fluorescence compared with those treated with free-NR. Increased cellular uptake of NR/GA-PEG-PLGA and NR/PEG-PLGA NPs was attributed to energy-dependent active transportation rather than the passive diffusion of free-NR. In addition, the encapsulation of NR in NPs could easily avoid its excretion from cells. At all time-points, the fluorescence intensity was significantly higher in the GA-coated NP groups than in the non-GA-coated groups. Of note, similar results were also observed in A549 cells, indicating that the affinity of

GA modification for liver cancer cells was not significantly different between these two types of cells. This suggests that the experimental design may need to be improved. Next, the cellular internalization of GA-modified NPs into HepG2 cells was examined using a CLSM. Both NP groups exhibited higher levels of NR cellular internalization compared with the free-NR group (Fig. 2). The uptake of GA-coated NPs was higher than that of nano GA-coated NPs in the cytoplasm and nucleus of HepG2 cells, suggesting that GA decoration was effective in delivering drugs to cells with high GA receptor expression. In accordance with the FCM data, these results demonstrated that GA receptor-mediated endocytosis efficiently and selectively transmits GA-coated NPs to HepG2 cells, thus improving targeted drug delivery to tumour tissues.

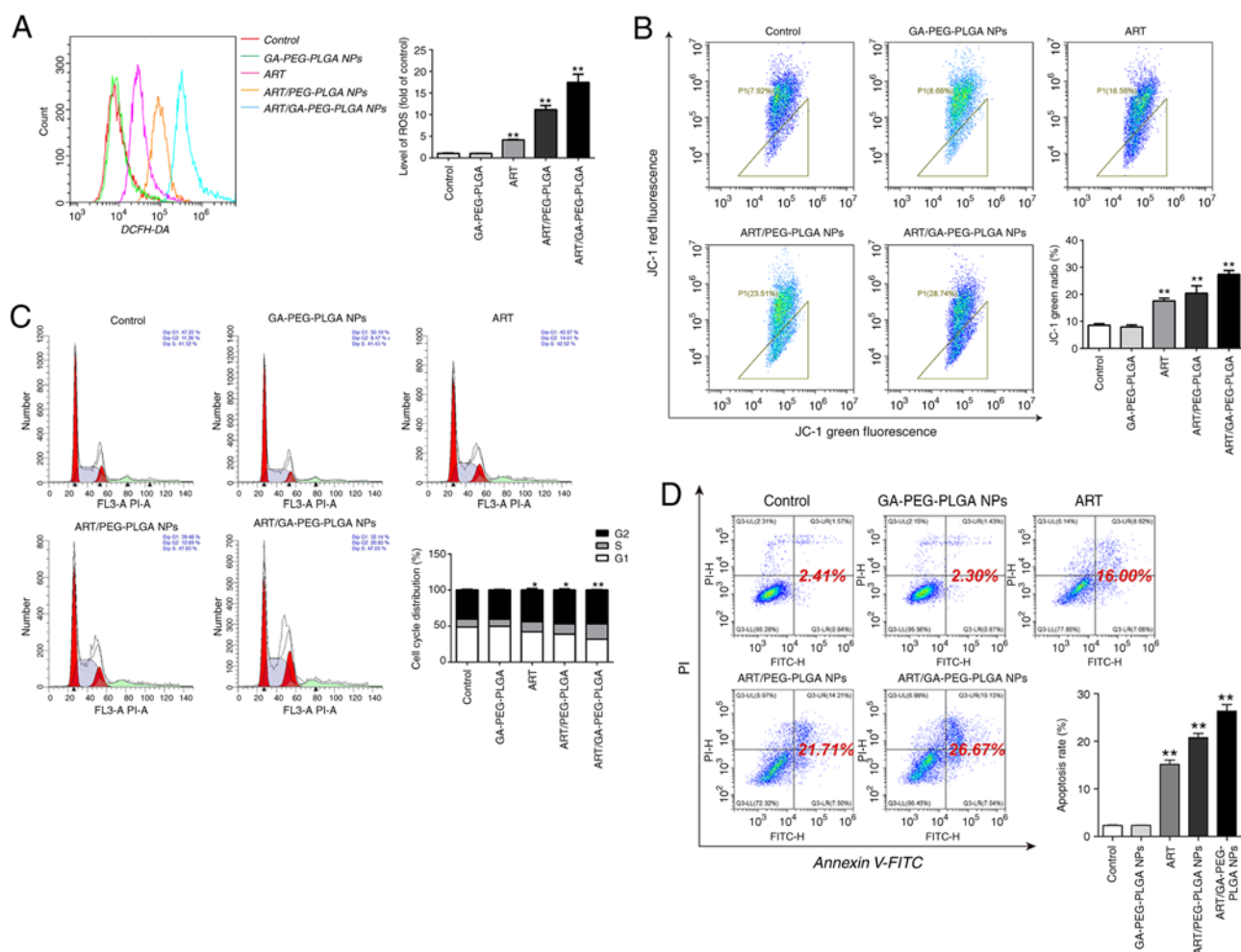


Figure 3. Effects of the different formulations on ROS production in HepG2 cells. (A) ROS levels were measured using a DCFH-DA probe. (B) Effect of the different formulations on the mitochondrial membrane potential in HepG2 cells. (C) ART inhibited the growth of HepG2 cells by inducing S phase arrest. (D) Flow cytometry of propidium iodide stained HepG2 cells. Effects of the different formulations on the apoptosis rate of HepG2 cells. HepG2 cells were treated with the different formulations, and the cell apoptosis in the indicated groups was measured via FCM after 72 h. The results are presented as the mean \pm SD (n=3). *P<0.05 and **P<0.01 vs. the control group. ROS, reactive oxygen species; DCFH-DA, 2',7'-dichlorodihydrofluorescein diacetate; ART, artesunate; GA, glycyrrhetic acid; NPs, liver-targeted nanoparticles; PEG-PLGA, polyethylene glycol-poly (lactic-co-glycolic acid).

Various endocytic inhibitors were employed to probe the internalization channels of GA-coated NPs. The significantly lower uptake observed following 2-deoxyglucose exposure indicated that it was relevant to the energy-dependent process of endocytosis (Fig. 1C). Pre-incubation with wortmannin, genistein and methyl- β -cyclodextrin significantly inhibited the intracellular uptake of NPs, suggesting that the macropinocytosis and caveolae-mediated pathways were the internalization channels. In comparison, the chlorpromazine-treated group exhibited no significant decline in NP uptake, indicating that the specific clathrin-mediated pathway was not the uptake pathway in this case. Hence, micropinocytosis and caveolae-mediated endocytosis were the internalization channels of the GA-modified NPs. In addition, the uptake of GA-coated NPs was significantly reduced by free-GA pre-treatment through a competitive combination of the GA receptors. Surplus free-GA can saturate these binding sites, ensuring that the GA-coated NPs can no longer utilize them. The results revealed that the uptake of GA-coated NPs by liver cancer cells depend largely on these GA-binding sites.

Pro-apoptotic effects of ART/GA-PEG-PLGA NPs and the underlying mechanisms. The cells were incubated with blank NPs or other formulations at an ART concentration of 5 mg/ml. Compared with normal cells, blank NP-treated cells exhibited no change in intracellular ROS levels, indicating that the blank NPs demonstrate favorable biocompatibility (Fig. 3A). ART-loaded NPs triggered a higher ROS level than free-ART. Moreover, compared with none-GA-modified NPs, the GA-modified NPs exhibited higher ROS levels. This increase in ROS levels resulted in cell growth arrest and apoptosis. These data demonstrated that the GA-coated NPs were superior to normal NPs in causing oxidative damage to liver cancer cells.

The mitochondrial membrane potential (MMP) is an important parameter for mitochondrial function and its decrease is often considered to promote apoptosis. An increase in the green fluorescence ratio indicates the occurrence of mitochondrial depolarization. It was observed that blank NPs did not affect the MMP, whereas the ART-loaded NPs decreased it in the HepG2 cells (Fig. 3B). The levels of the JC-1 green ratio were significantly increased in the HepG2

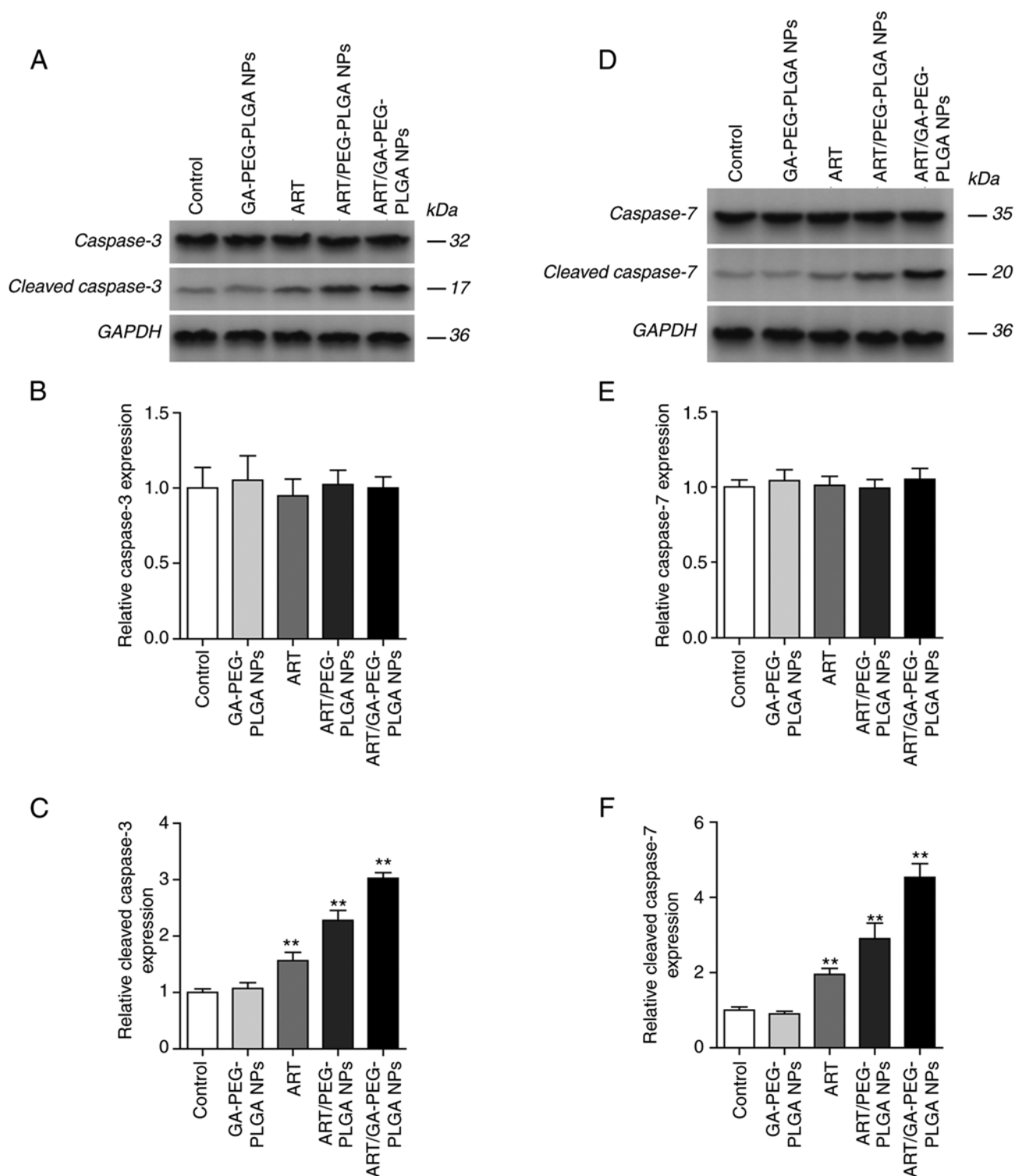


Figure 4. Effect of the different formulations on caspase-3, cleaved caspase-3, caspase-7, and cleaved caspase-7 activities in HepG2 cells. HepG2 cells were treated with the different formulations for 72 h. The activities of (A and B) caspase-3, (A and C) cleaved caspase-3, (D and E) caspase-7 and (D and F) cleaved caspase-7 were detected via western blotting. The results are presented as the mean \pm standard deviation (n=3). **P<0.01 vs. the control group. ART, artesunate; GA, glycyrrhetic acid; NPs, liver-targeted nanoparticles; PEG-PLGA, polyethylene glycol-poly (lactic-co-glycolic acid).

cells following GA-coated NPs treatment compared with that in the cells treated with non-GA-coated NPs.

The effects of ART/GA-PEG-PLGA NPs on cell cycle progression in the HepG2 cells were assessed via FCM. The ART formulations induced cell cycle arrest in the HepG2 cells and not in the untreated or blank NP-treated cells (Fig. 3C). The cell distribution decreased in the G1 phase and

increased in the S and G2 phases following the treatment. In all the preparations, the ART/GA-PEG-PLGA NPs exhibited the strongest effect on cell cycle inhibition in the S phase. Therefore, these results suggested that ART/GA-PEG-PLGA NPs can effectively inhibit HepG2 cell proliferation.

In the present study, the effects of ART-loaded NPs on apoptosis in HepG2 cells were assessed. Following culture,

Table I. Pharmacokinetic parameters in rats treated with a free-ART suspension or ART-loaded NPs at an equivalent dose of 5 mg ART per kg (n=3).

Groups	Parameters					
	C _{max}	T _{max}	AUC _{0-t} , h/ng/ml	AUC _{0-∞} , h/ng/ml	MRT, h	T1/2z, h
ART	4,578	0.25	2,539.49	2,539.54	0.50	0.25
ART/GA-PEG-PLGA NPs	3,897	0.25	12,527.96 ^a	13,477.30 ^a	5.54 ^a	6.67 ^a

^aP<0.01 vs. the ART group. AUC, area under the curve; MRT, mean retention time; ART/GA-PEG-PLGA NPs, artesunate-glycyrrhetic acid-coated polyethylene glycol-poly (lactic-co-glycolic acid) liver-targeted nanoparticles.

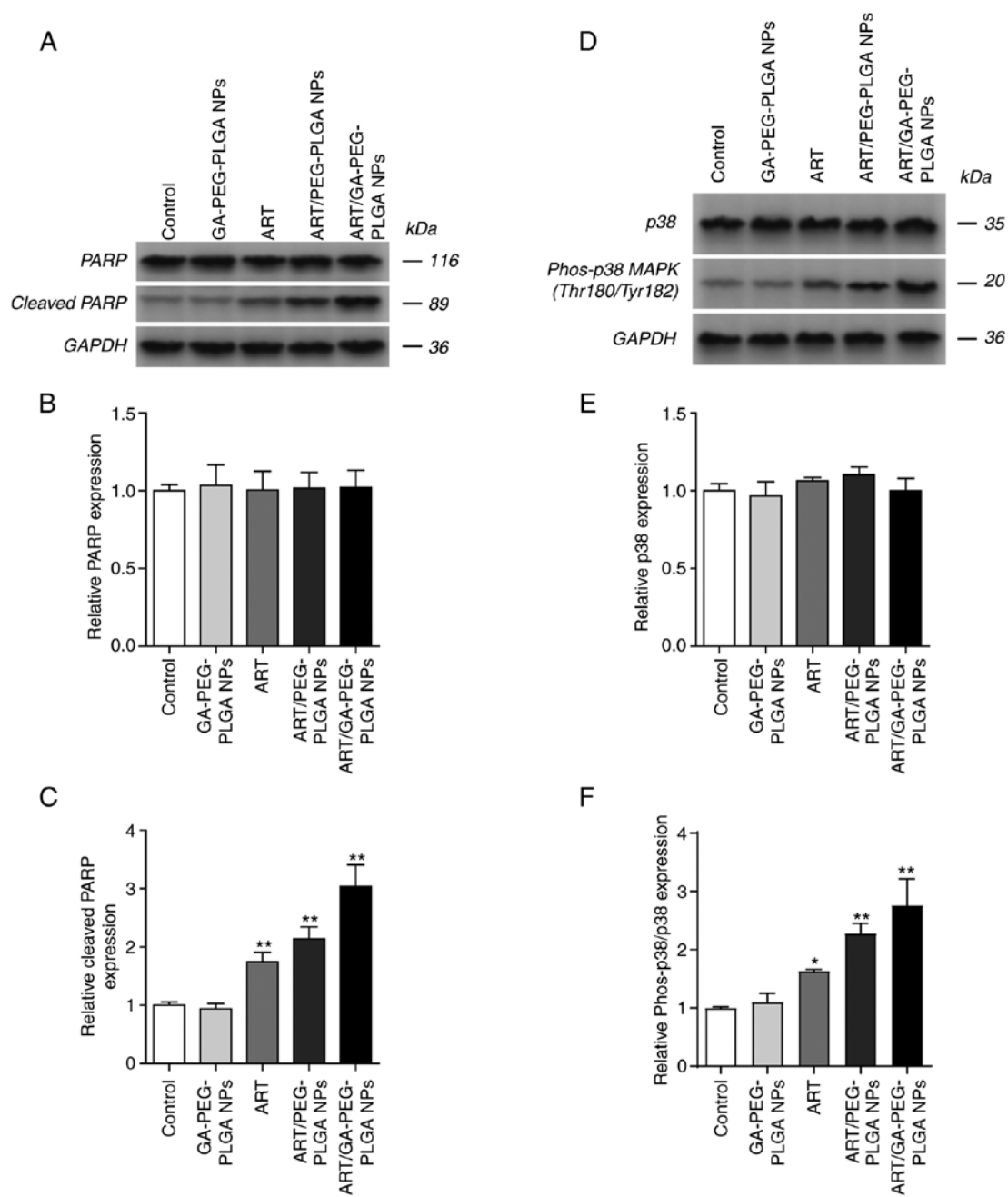


Figure 5. Effects of the different formulations on PARP, cleaved PARP, p38 and Phos-p38 MAPK (Thr180/tyr182) expression in HepG2 cells. HepG2 cells were treated with the different formulations for 72 h. The expression of (A and B) PARP, (A and C) cleaved PARP, (D and E) p-38 and (D and F) Phos-p38 MAPK (Thr180/tyr182) was detected via western blotting. The results are presented as the mean ± standard deviation (n=3). *P<0.05 and **P<0.01 vs. the control group. PARP, poly (ADP-Ribose)-polymerase; ART, artesunate; GA, glycyrrhetic acid; NPs, liver-targeted nanoparticles; PEG-PLGA, polyethylene glycol-poly (lactic-co-glycolic acid).

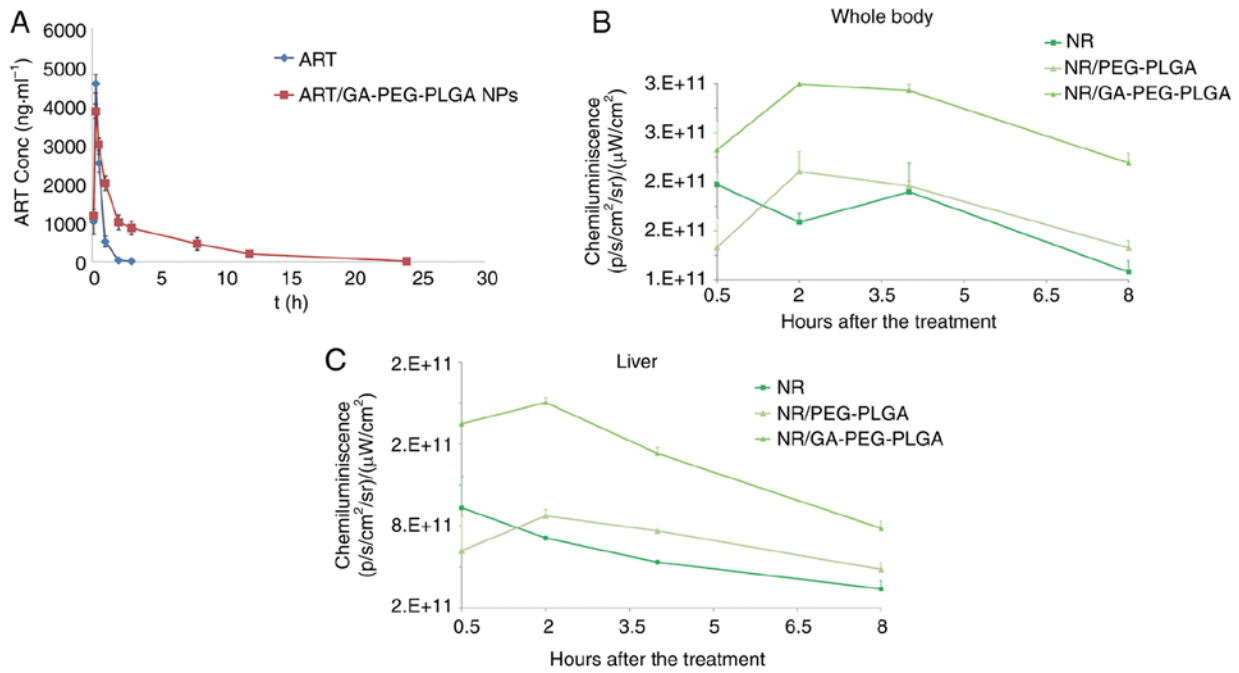


Figure 6. Pharmacokinetic profiles of ART in SD rats following the intragastrical administration of free-ART or ART-loaded NPs at an equivalent dose of 50 mg ART per kg (n=3). (A) ART was extracted from plasma and measured via LC/MS/MS. (B and C) Tumour bioluminescence curve in a Hep3b-luc orthotopic xenograft model following the administration of the different formulations. ART, artesunate; GA, glycyrrhetic acid; NPs, liver-targeted nanoparticles; PEG-PLGA, polyethylene glycol-poly (lactic-co-glycolic acid).

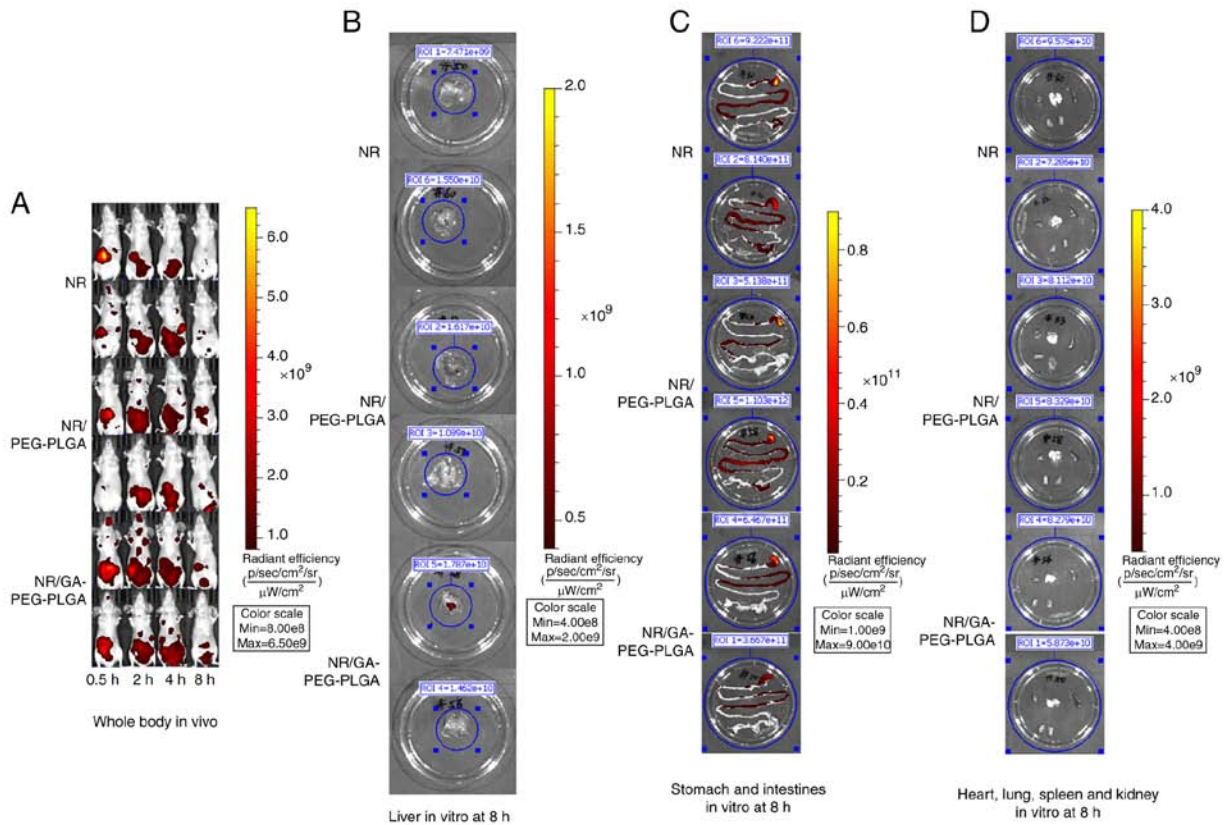


Figure 7. Fluorescence signal distribution in the whole body at 0.5, 2, 4 and 8 h and in the main organs at 8 h *in vitro* (n=2). NR was used as the fluorescent probe to detect the hepatoma-targeting ability and bio-distribution of GA-PEG-PLGA NPs. The tumour model mice were randomized into three groups and administered intragastrically the different NR preparations at an NR dose of 20 mg/kg. The mice were euthanized after 8 h, the main organs (heart, liver, spleen, lungs and kidneys) were dissected and the NR signal intensity in each organ was detected. Compared with the NR-loaded NP group, the free-NR group exhibited lower fluorescence levels at 2 h after drug administration. Higher levels of NR were observed in the NR-loaded NP groups at 2, 4 and 8 h compared with the free-NR treated group in the whole body and liver. The liver fluorescence of NR in the GA-modified NP group was remarkably higher than that observed in the non-GA-modified group (P<0.05). Fluorescence of the (A) whole body; (B) liver; (C) stomach and intestine; and (D) heart, spleen, lungs and kidneys. NR, Nile red; GA, glycyrrhetic acid; NPs, liver-targeted nanoparticles; PEG-PLGA, polyethylene glycol-poly (lactic-co-glycolic acid).

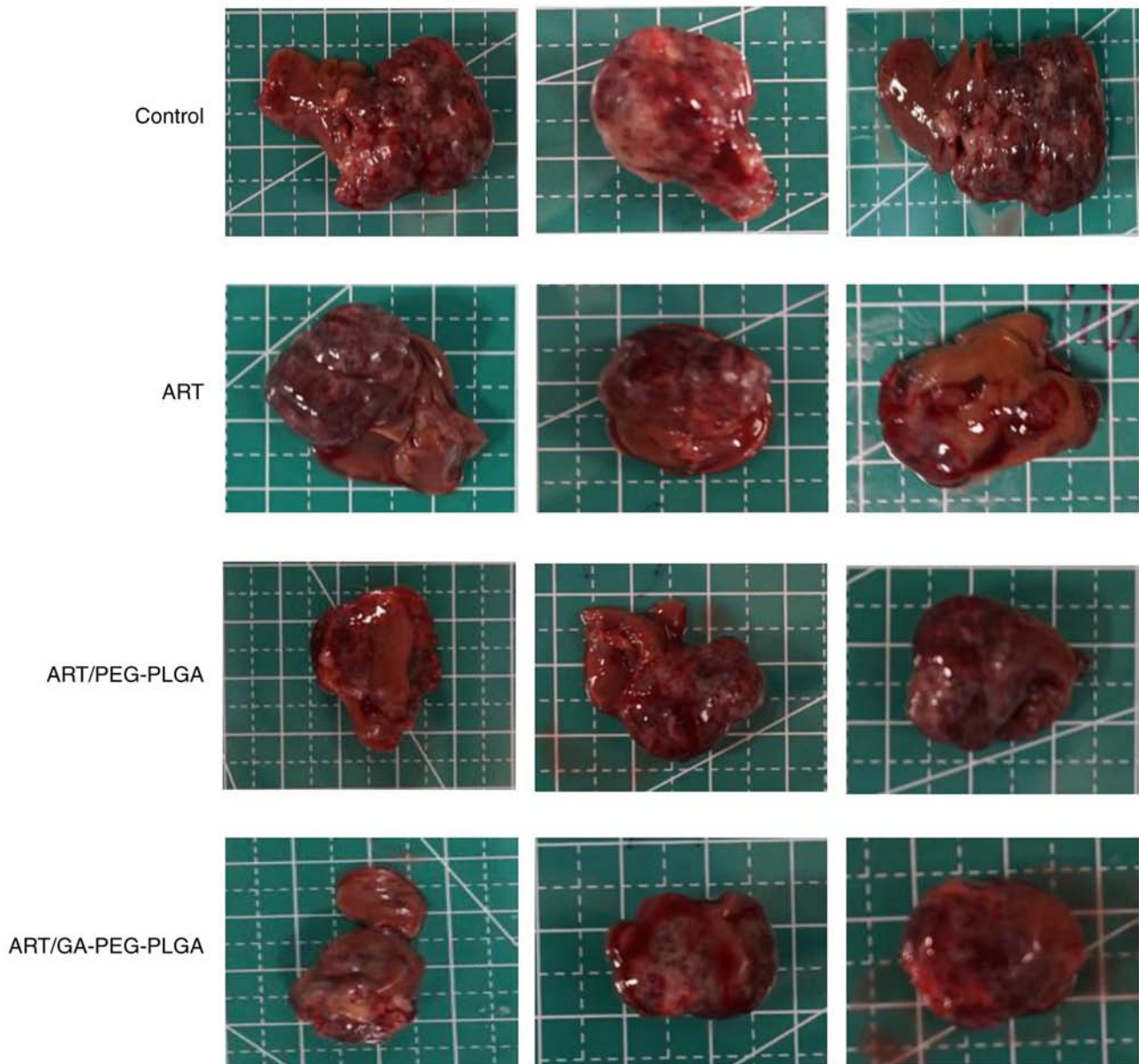


Figure 8. Tumours removed from each group. Mice bearing Hep3B-luc in situ transplanted tumours were randomized into four groups (i.e., control, free-NR, NR/PEG-PLGA NPs and NR/GA-PEG-PLGA NPs) and treated intragastrically with different ART preparations at an ART concentration of 50 mg/kg once daily for 24 days, with the exception of the control group. The tumours were collected at 4 h after the last drug administration. The distance between the solid lines, the solid lines and the dashed lines on the anatomical board is 1 cm and 0.5 cm, respectively. NR, Nile red; GA, glycyrrhetic acid; NPs, liver-targeted nanoparticles; PEG-PLGA, polyethylene glycol-poly (lactic-co-glycolic acid); ART, artesunate.

cellular apoptosis was determined via Annexin V-FITC and PI double staining. ART-loaded NPs exhibited significantly stronger apoptosis-inducing effects on HepG2 cells than free-ART; moreover, compared with the other groups, ART/GA-PEG-PLGA NP-treated HepG2 cells exhibited the highest apoptotic rate (Fig. 3D). These data indicated that ART/GA-PEG-PLGA NPs demonstrated promising apoptotic effects in the HepG2 cells.

Western blot analyses revealed that ART-loaded NPs induced internal apoptosis pathways in HepG2 cells (Figs. 4 and 5). Caspase-3/7 is directly involved in the cleavage of important intracellular substrates to disintegrate cellular structures during apoptosis (44). P38 reportedly functions as an antitumour factor and regulates the cell cycle at several

transition points (45). PARP is related to cell death and is cleaved specifically and rapidly during apoptosis (46,47). Compared with the free-ART group and ART/PEG-PLGA NP group, cleaved caspase-3/7 expression increased following treatment with ART/GA-PEG-PLGA NPs (Fig. 4C and F), whereas negligible variation was observed for caspase-3/7 expression (Fig. 4B and E). Furthermore, ART/GA-PEG-PLGA NPs notably upregulated cleaved PARP and Phos-p38/p38 MAPK (Thr180/tyr182) in HepG2 cells compared with free-ART and ART/PEG-PLGA NPs (Fig. 5C and F), whereas negligible variation was observed for PARP and p38 MAPK (Thr180/tyr182) expression (Fig. 5B and E). Similar outcomes were obtained in the cell apoptosis assay. Because p38 MAPK is an important modulator of cell death, increased cell apoptosis triggered by

Table II. Therapeutic effects in the Hep3B-luc xenograft model.

Group	Bioluminescence (ROI, $\times 10^9$ photons/sec) (PG-21)	IRT _{Bioluminescence} , %	Tumour weight, g	IRT _{Tumour weight} , %
Control	5.72 \pm 1.38	-	3.78 \pm 0.15	-
ART	4.49 \pm 0.55	21.50	30.3 \pm 0.36 ^a	19.84
ART/PEG-PLGA NPs	2.94 \pm 0.37 ^{a,b}	48.60	1.92 \pm 0.23 ^{a,c}	49.21
ART/GA-PEG-PLGA NPs	1.03 \pm 0.29 ^{a,c,d}	81.99	0.74 \pm 0.11 ^{a,c,d}	80.42

^aP<0.01 vs. the control group; ^bP<0.05, ^cP<0.01 vs. the ART group; ^dP<0.01 vs. the ART/PEG-PLGA group. ROI, region of interest; IRT, inhibition rate of tumour; ART/GA-PEG-PLGA NPs, artesunate-glycyrrhetic acid-coated polyethylene glycol-poly (lactic-co-glycolic acid) liver-targeted nanoparticles.

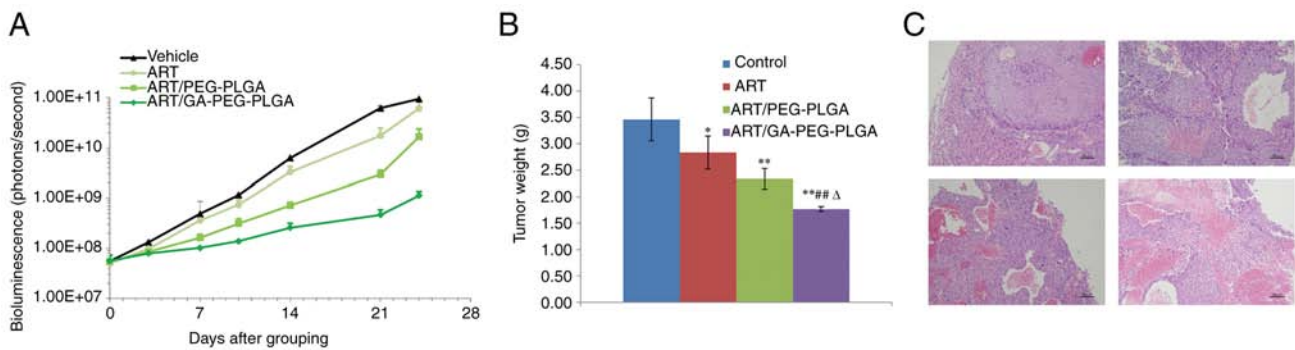


Figure 9. *In vivo* antitumour effects of the ART formulations on a xenograft tumour model with Hep3B-luc cell implantation. (A-C) Panels depicting the (A) Bioluminescence, (B) tumour weight and (C) haematoxylin and eosin staining of the tumour sections of mice that received intragastric administration of saline, free-ART, ART/PEG-PLGA NPs or ART/GA-PEG-PLGA NPs (n=3). *P<0.05 and **P<0.01 vs. the control group; ##P<0.01 vs. the free-ART group; ^aP<0.05 vs. the ART/PEG-PLGA NP group). ART, artesunate; GA, glycyrrhetic acid; NPs, liver-targeted nanoparticles; PEG-PLGA, polyethylene glycol-poly (lactic-co-glycolic acid).

ART/GA-PEG-PLGA NPs is considered to be mediated by the p38 MAPK/caspase-3/7 signaling pathway.

Pharmacokinetics studies. Following drug administration, a sharp increase and then a sharp decrease in the plasma concentrations of ART was observed in the free-ART group. ART was almost undetectable at 3 h following drug intragastric administration (Fig. 6A). Conversely, the ART cycles were longer in the ART/GA-PEG-PLGA NP group than in the free-ART group, and its plasma concentrations could still be detected at 12 h after drug administration. There was a large difference in the time courses of plasma ART concentrations between the free-ART and GA-coated NP groups, indicating that nanorization could prolong the peripheral circulation of ART. The main pharmacokinetics parameters of free-ART and ART-loaded NPs are summarized in Table I. The total area under the curve ($AUC_{0-\infty}$) of the ART-loaded NP group was significantly greater than that of the free-ART group, indicating that bioavailability was enhanced after the encapsulation of ART in NPs. The extended mean retention time (MRT) and elimination half-life ($t_{1/2z}$) of ART-loaded NPs contributed to the higher $AUC_{0-\infty}$ values. Interestingly, the pharmacokinetic parameters of the ART/GA-PEG-PLGA NP group were different from those of the free-ART group. Although the C_{max} of the NP group was lower than that of the free-ART group, its $AUC_{0-\infty}$ value and MRT were higher than

those of the free-ART group. It was hypothesized that these results could be attributed to the liver-targeting feature of ART/GA-PEG-PLGA NPs, which promoted the liver accumulation of ART and decreased its level in the blood circulation.

Hepatoma-targeting and bio-distribution of GA-coated NPs. The fluorescence signal distribution of NR was analysed in the whole body and liver at different time-points (Figs. 6B and C and 7). Compared with the NR-loaded NP group, the free-NR group exhibited lower fluorescence levels at 2 h following the drug administrations, implying that free-NR was eliminated faster *in vivo*. Although the NR levels of the free-NR-treated group were higher than those of the NR/PEG-PLGA group at 0.5 h, higher levels of NR were observed in the NR-loaded NP groups at 2, 4 and 8 h in the whole body and liver. The liver fluorescence of NR in the GA-modified NP group was markedly higher than that detected in the non-GA-modified group, suggesting that GA modification upregulated the liver-targeting effect of the NPs. Thus, these data demonstrated that GA-PEG-PLGA NPs can promote the liver-targeting distribution of the drug and prolong its retention time.

Antitumour activity. A xenograft tumour model was generated in BALB/c nude mice with Hep3B-luc cell embedment, to explore the antitumour abilities of ART/GA-PEG-PLGA NPs.

Tumours removed from each group are presented in Fig. 8. The tumour growth, weight and survival curves of each group were recorded and calculated (Fig. 9A and B). Similar to patients with liver cancer, it was observed that tumour-bearing mice succumbed because of inadequate nutrition during long-term treatment, whereas no deaths were observed in the different ART formulation-treated groups during the test period. Following the completion of the experiment, the *in vitro* liver bioluminescence and tumour weight data revealed that the trend of the IRT according to the different ART formulations was ART/GA-PEG-PLGANPs > ART/PEG-PLGA NPs > free-ART (Table II). An additional analysis revealed that the IRT results of the NP and free-ART groups coincided in the two calculation approaches. In addition, a histological analysis of tumour sections revealed that compared with the other groups the tumour necrosis area was larger and apoptosis was increased in tumours treated with ART/GA-PEG-PLGA NPs (Fig. 9C). These outcomes revealed that ART/GA-PEG-PLGA NPs had a more promising antitumour activity than free-ART or ART-loaded non-functional NPs.

Discussion

Significant progress has been made in the nano-targeted delivery systems used for liver cancer treatment over the last two decades. However, NPs designed to target liver cancer continue facing certain challenges, such as the low effective concentration of drugs in tumour tissues (48), with a mediocre 4% passive targeted-drug delivery and 8% active targeted-drug delivery (49). These findings were mainly attributed to an elaborate reticuloendothelial system and the trapping and interference of NPs in the delivery pathway. Regarding active targeted delivery, although various ligands (such as peptides, antibodies and galactose) are currently in use (50), the possible immunoreaction of exogenous biomolecular targeting ligands and the instability of the galactose-targeting effect continue to hinder the efficiency of their delivery. Therefore, there remain high demands for novel liver cancer specific delivery targeting ligands. The emergence of GA renewed hope in this field since it not only yielded a higher expression of receptors on liver cancer cells but also exerted numerous pharmacological activities, such as anti-ulcer, anti-allergy, immune-modulating, antiviral, antitumour, liver-preservation and antioxidant effects, suggesting that the GA-coated NPs proposed in the present study could target hepatoma tissue, improve treatment outcomes and reduce adverse events.

Because of the generally serious toxicity of chemotherapeutics, the active ingredients of traditional Chinese medicine have become a hot topic in antitumour research as they reportedly possess various curative effects against tumour occurrence, development, metastasis and immune modulation via multiple ways and multi-targets (51). ART, an artemisinin derivative isolated from the traditional herb *Artemisia annua*, can induce the apoptosis and differentiation of various human tumour cells and is regarded as a potential anticancer agent (39,52,53). However, its clinical application is seriously affected due to the poor pharmaceutical properties aforementioned. In the present study, ART was encapsulated in GA-coated NPs to overcome the existing limitations and enhance its treatment effect.

The present data illustrated that the ART/GA-PEG-PLGA NPs could significantly increase the liver distribution of ART and prolong MRT to enhance its therapeutic effects compared with free-ART.

GA-modified DDSs have garnered considerable attention regarding the treatment of liver cancer. The main reasons for this include their capability of promoting GA receptor-mediated endocytosis and enhancing liver targeting. These observations are consistent with the present research results. Most studies regarding GA-modified DDSs used HepG2 cells to study *in vitro* cellular uptake (35,54-56), mainly for the following reasons: High GA receptor expression, high differentiation degree, relatively complete biotransformation characteristics of metabolic enzymes, retention of the stability of metabolic enzymes in studies related to drug effects (absence of changes caused by increased number of passages), and homology between the contained biotransformation metabolic enzymes and normal human liver parenchyma cells. In these studies that aimed at improving the cellular uptake of GA-modified DDSs, A549 cells are commonly used as a control because of their low GA receptor expression (50,55). Therefore, the present study also selected HepG2 and A549 cells to study the specific liver cancer-targeting function of the system and improve the cellular internalization of GA-modified NPs. The HepG2 cell line was authenticated before the study began.

Induction of apoptosis is one of the most important targets of cancer research; therefore, the pro-apoptotic effects of ART/GA-PEG-PLGA NPs and their possible underlying mechanisms were investigated. The pre-set results revealed that ART/GA-PEG-PLGA NPs remarkably increased cell apoptosis by enhancing cellular uptake mediated by the GA ligand. As expected, the *in vivo* antitumour effects were consistent with the *in vitro* results (40), indicating the potent anti-liver cancer efficiency of ART/GA-PEG-PLGA NPs.

Of note, the present study also has certain shortcomings. Due to limited research funding, insufficient research samples and short research time, there are shortcomings in the reliability and universality of the study's conclusions. In future research, we will improve new research methods, such as using gene knockout technology to prepare GA receptor knockout HepG2 cells, to even out these shortcomings and improve the quality and reliability of the research.

In the present study, innovative hepatoma-targeting ART-loaded and GA-coated PEG-PLGA NPs were successfully developed to deliver ART to hepatoma cells. GA modification enabled the selective delivery to and the accumulation of ART in liver cells. ART/GA-PEG-PLGA NPs exhibited improved tumour-targeting abilities and *in vivo* treatment efficiency, which were attributed to the tumour-targeting ability exhibited by GA. Overall, ART/GA-PEG-PLGA NPs may have promising prospects for treating hepatoma.

Acknowledgements

Not applicable.

Funding

The present study was supported by the National Natural Science Foundation of China (grant no. 82104699), the

Research Project on the Application of Public Welfare Technology supported by the Science and Technology Department of Zhejiang (grant no. LGF22H290003), the Medical Health Science and Technology Major Project of Hangzhou Health Commission (grant no. Z20230014) and the Hepatology (Traditional Chinese and Western Medicine) of Hangzhou Medical Peak Subject.

Availability of data and materials

All data generated or analyzed during this study are included in this published article.

Authors' contributions

XWP, JSH, SRL, RXZ and JFB participated in research design. XWP, JJX, YDS, RYH and TTS conducted experiments. YDS, RYH and TTS contributed reagents or analytic tools. XWP, JJX, YDS, RYH, RXZ and JFB performed data analysis. XWP, JSH, SRL, RXZ and JFB discussed and edited the manuscript. XWP, JJX and YDS wrote or contributed to the writing of the manuscript. All authors have read and approved the final version of the manuscript. JJX and YDS confirm the authenticity of all the raw data.

Ethics approval and consent to participate

All procedures performed in studies involving animal participants were in accordance with the national ethical standards. The present study was approved (approval no. ON-01-QD003-2020v1.0) by the Institutional Animal Care and Use Committee of WuXi AppTec (Nantong) Co., Ltd.

Patient consent for publication

Not applicable.

Competing interests

The authors declare that they have no competing interests.

References

- Sung H, Ferlay J, Siegel RL, Laversanne M, Soerjomataram I, Jemal A and Bray F: Global cancer statistics 2020: GLOBOCAN estimates of incidence and mortality worldwide for 36 cancers in 185 countries. *CA Cancer J Clin* 71: 209-249, 2021.
- Zhou M, Wang H, Zeng X, Yin P, Zhu J, Chen W, Li X, Wang L, Wang L, Liu Y, *et al*: Mortality, morbidity, and risk factors in China and its provinces, 1990-2017: A systematic analysis for the global burden of disease study 2017. *Lancet* 394:1145-1158, 2019.
- Kulik L and El-Serag HB: Epidemiology and management of hepatocellular carcinoma. *Gastroenterology* 156: 477-491.e1, 2019.
- Sugawara Y and Hibi T: Surgical treatment of hepatocellular carcinoma. *Biosci Trends* 15: 138-141, 2021.
- Piñero F, Silva M and Iavarone M: Sequencing of systemic treatment for hepatocellular carcinoma: Second line competitors. *World J Gastroenterol* 26: 1888-1900, 2020.
- Colquhoun SD and Wan YY: Hepatocellular carcinoma diagnosis and treatment: An overview. *Liver Res* 4: 159-160, 2020.
- Yang JD and Heimbach JK: New advances in the diagnosis and management of hepatocellular carcinoma. *BMJ* 371: m3544, 2020.
- Malla RR, Kumari S, Kkg D, Momin S and Nagaraju GP: Nanotheranostics: Their role in hepatocellular carcinoma. *Crit Rev Oncol Hematol* 151: 102968, 2020.
- Wiwachitawee K, Quarterman JC, Geary SM and Salem AK: Enhancement of therapies for glioblastoma (GBM) using nanoparticle-based delivery systems. *AAPS PharmSciTech* 22: 71, 2021.
- Kalyane D, Raval N, Maheshwari R, Tambe V, Kalia K and Tekade RK: Employment of enhanced permeability and retention effect (EPR): Nanoparticle-based precision tools for targeting of therapeutic and diagnostic agent in cancer. *Mater Sci Eng C Mater Biol Appl* 98: 1252-1276, 2019.
- Yang C, Tan Y, Qi H, Zhou J, Long L, Zhan Q, Wang Y, Yuan X and Kang C: Boosting of the enhanced permeability and retention effect with nanocapsules improves the therapeutic effects of cetuximab. *Cancer Biol Med* 17: 433-443, 2020.
- Yang M, Li J, Gu P and Fan X: The application of nanoparticles in cancer immunotherapy: Targeting tumor microenvironment. *Bioact Mater* 6: 1973-1987, 2020.
- Baker A, Khan MS, Iqbal MZ and Khan MS: Tumor-targeted drug delivery by nanocomposites. *Curr Drug Metab* 21: 599-613, 2020.
- Hu X, Zhang J, Deng L, Hu H, Hu J and Zheng G: Galactose-modified pH-sensitive niosomes for controlled release and hepatocellular carcinoma target delivery of tanshinone IIA. *AAPS PharmSciTech* 22: 96, 2021.
- Severino P, da Silva CF, Andrade LN, de Lima Oliveira D, Campos J and Souto EB: Alginate nanoparticles for drug delivery and targeting. *Curr Pharm Des* 25: 1312-1334, 2019.
- Wathoni N, Rusdin A, Motoyama K, Joni IM, Lesmana R and Muchtaridi M: Nanoparticle drug delivery systems for α -mangostin. *Nanotechnol Sci Appl* 13: 23-36, 2020.
- Essa D, Kondiah PPD, Choonara YE and Pillay V: The design of poly (lactide-co-glycolide) nanocarriers for medical applications. *Front Bioeng Biotechnol* 8: 48, 2020.
- Begines B, Ortiz T, Pérez-Aranda M, Martínez G, Merinero M, Argüelles-Arias F and Alcludia A: Polymeric nanoparticles for drug delivery: Recent developments and future prospects. *Nanomaterials (Basel)* 10: 1403, 2020.
- Du M, Ouyang Y, Meng F, Zhang X, Ma Q, Zhuang Y, Liu H, Pang M, Cai T and Cai Y: Polymer-lipid hybrid nanoparticles: A novel drug delivery system for enhancing the activity of Psoralen against breast cancer. *Int J Pharm* 561: 274-282, 2019.
- Anderson CF, Grimmert ME, Domalewski CJ and Cui H: Inhalable nanotherapeutics to improve treatment efficacy for common lung diseases. *Wiley Interdiscip Rev Nanomed Nanobiotechnol* 12: e1586, 2020.
- Carter P, Narasimhan B and Wang Q: Biocompatible nanoparticles and vesicular systems in transdermal drug delivery for various skin diseases. *Int J Pharm* 555: 49-62, 2019.
- Wei T, Cheng Q, Min YL, Olson EN and Siegwart DJ: Systemic nanoparticle delivery of CRISPR-Cas9 ribonucleoproteins for effective tissue specific genome editing. *Nat Commun* 11: 3232, 2020.
- Anselmo AC and Mitragotri S: Nanoparticles in the clinic: An update. *Bioeng Transl Med* 4: e10143, 2019.
- Krauss AC, Gao X, Li L, Manning ML, Patel P, Fu W, Janoria KG, Gieser G, Bateman DA, Przepiorka D, *et al*: FDA approval summary: (Daunorubicin and Cytarabine) Liposome for injection for the treatment of adults with high-risk acute myeloid leukemia. *Clin Cancer Res* 25: 2685-2690, 2019.
- Naqvi S, Panghal A and Flora SJS: Nanotechnology: A promising approach for delivery of neuroprotective drugs. *Front Neurosci* 14: 494, 2020.
- Gu Z, Wang Q, Shi Y, Huang Y, Zhang J, Zhang X and Lin G: Nanotechnology-mediated immunochemotherapy combined with docetaxel and PD-L1 antibody increase therapeutic effects and decrease systemic toxicity. *J Control Release* 286: 369-380, 2018.
- Chen B, Dai W, He B, Zhang H, Wang X, Wang Y and Zhang Q: Current multistage drug delivery systems based on the tumor microenvironment. *Theranostics* 7: 538-558, 2017.
- Zhang YR, Lin R, Li HJ, He WL, Du JZ and Wang J: Strategies to improve tumor penetration of nanomedicines through nanoparticle design. *Wiley Interdiscip Rev Nanomed Nanobiotechnol* 11: e1519, 2019.
- Niu Y, Zhu J, Li Y, Shi H, Gong Y, Li R, Huo Q, Ma T and Liu Y: Size shrinkable drug delivery nanosystems and priming the tumor microenvironment for deep intratumoral penetration of nanoparticles. *J Control Release* 277: 35-47, 2018.

30. Lim S, Park J, Shim MK, Um W, Yoon HY, Ryu JH, Lim DK and Kim K: Recent advances and challenges of repurposing nanoparticle-based drug delivery systems to enhance cancer immunotherapy. *Theranostics* 9: 7906-7923, 2019.
31. Gonda A, Zhao N, Shah JV, Calvelli HR, Kantamneni H, Francis NL and Ganapathy V: Engineering tumor-targeting nanoparticles as vehicles for precision nanomedicine. *Med One* 4: e190021, 2019.
32. Negishi M, Irie A, Nagata N and Ichikawa A: Specific binding of glycyrrhetic acid to the rat liver membrane. *Biochim Biophys Acta* 1066: 77-82, 1991.
33. Sun Y, Dai C, Yin M, Lu J, Hu H and Chen D: Hepatocellular carcinoma-targeted effect of configurations and groups of glycyrrhetic acid by evaluation of its derivative-modified liposomes. *Int J Nanomedicine* 13: 1621-1632, 2018.
34. Wu F, Li X, Jiang B, Yan J, Zhang Z, Qin J, Yu W and Gao Z: Glycyrrhetic acid functionalized nanoparticles for drug delivery to liver cancer. *J Biomed Nanotechnol* 14: 1837-1852, 2018.
35. Li YL, Zhu XM, Liang H, Orvig C and Chen ZF: Recent advances in asialoglycoprotein receptor and glycyrrhetic acid receptor-mediated and/or pH-responsive hepatocellular carcinoma-targeted drug delivery. *Curr Med Chem* 28: 1508-534, 2021.
36. Stecanella LA, Bitencourt APR, Vaz GR, Quarta E, Silva Júnior JOC and Rossi A: Glycyrrhetic acid and its hydrolyzed metabolite 18 β -glycyrrhetic acid as specific ligands for targeting nanosystems in the treatment of liver cancer. *Pharmaceutics* 13: 1792, 2021.
37. Kim J, Lee S and Na K: Glycyrrhetic acid-modified silicon phthalocyanine for liver cancer-targeted photodynamic therapy. *Biomacromolecules* 22: 811-822, 2021.
38. Li L, Han S, Yang C, Liu L, Zhao S, Wang X, Liu B, Pan H and Liu Y: Glycyrrhetic acid modified MOFs for the treatment of liver cancer. *Nanotechnology* 31: 325602, 2020.
39. Huang S, Ren D, Wu X, Li M, Yu X, Nie X, Wang Y and Wang Y: Glycyrrhetic acid and TAT peptide modified dual-functional liposomes for treatment of hepatocellular cancer. *Curr Top Med Chem* 20: 2493-2505, 2020.
40. Li ZJ, Dai HQ, Huang XW, Feng J, Deng JH, Wang ZX, Yang XM, Liu YJ, Wu Y, Chen PH, *et al.*: Artesunate synergizes with sorafenib to induce ferroptosis in hepatocellular carcinoma. *Acta Pharmacol Sin* 42: 301-310, 2021.
41. Yin S, Yang H, Zhao X, Wei S, Tao Y, Liu M, Bo R and Li J: Antimalarial agent artesunate induces G0/G1 cell cycle arrest and apoptosis via increasing intracellular ROS levels in normal liver cells. *Hum Exp Toxicol* 39: 1681-1689, 2020.
42. Pan X, Liu S, Ju L, Xi J, He R, Zhao Y, Zhuang R and Huang J: Preparation, evaluation, and in vitro cytotoxicity studies of artesunate-loaded glycyrrhetic acid decorated PEG-PLGA nanoparticles. *Drug Dev Ind Pharm* 46: 1889-1897, 2020.
43. Ye RR, Peng W, Chen BC, Jiang N, Chen XQ, Mao ZW and Li RT: Mitochondria-targeted artesunate conjugated cyclometalated iridium(III) complexes as potent anti-HepG2 hepatocellular carcinoma agents. *Metallomics* 12: 1131-1141, 2020.
44. McComb S, Chan PK, Guinot A, Hartmannsdottir H, Jenni S, Dobay MP, Bourquin JP and Bornhauser BC: Efficient apoptosis requires feedback amplification of upstream apoptotic signals by effector caspase-3 or -7. *Sci Adv* 5: eaau9433, 2019.
45. Martínez-Limón A, Joaquín M, Caballero M, Posas F and de Nadal E: The p38 pathway: From biology to cancer therapy. *Int J Mol Sci* 21: 1913, 2020.
46. Slade D: PARP and PARG inhibitors in cancer treatment. *Genes Dev* 34: 360-394, 2020.
47. Zhu H, Wei M, Xu J, Hua J, Liang C, Meng Q, Zhang Y, Liu J, Zhang B, Yu X and Shi S: PARP inhibitors in pancreatic cancer: Molecular mechanisms and clinical applications. *Mol Cancer* 19: 49, 2020.
48. Wilhelm S, Tavares AJ, Qin D, Ohta S, Audet J, Dvorak HF and Chan WCW: Analysis of nanoparticle delivery to tumours. *Nat Rev Mater* 1: 16014, 2016.
49. von Maltzahn G, Park JH, Lin KY, Singh N, Schwöppe C, Mesters R, Berdel WE, Ruoslahti E, Sailor MJ and Bhatia SN: Nanoparticles that communicate in vivo to amplify tumour targeting. *Nat Mater* 10: 545-552, 2011.
50. Chen F, Zhang J, He Y, Fang X, Wang Y and Chen M: Glycyrrhetic acid-decorated and reduction-sensitive micelles to enhance the bioavailability and anti-hepatocellular carcinoma efficacy of tanshinone IIA. *Biomater Sci* 4: 167-182, 2016.
51. Rahman M, Almalki WH, Alrobaian M, Iqbal J, Alghamdi S, Alharbi KS, Alruwaili NK, Hafeez A, Shaharyar A, Singh T, *et al.*: Nanocarriers-loaded with natural actives as newer therapeutic interventions for treatment of hepatocellular carcinoma. *Expert Opin Drug Deliv* 18: 489-513, 2021.
52. Yang X, Zheng Y, Liu L, Huang J, Wang F and Zhang J: Progress on the study of the anticancer effects of artesunate. *Oncol Lett* 22: 750, 2021.
53. Zhao F, Vakhrusheva O, Markowitsch SD, Slade KS, Tsaour I, Cinatl J Jr, Michaelis M, Efferth T, Haferkamp A and Juengel E: Artesunate impairs growth in cisplatin-resistant bladder cancer cells by cell cycle arrest, apoptosis and autophagy induction. *Cells* 9: 2643, 2020.
54. Zhao L, Liang L, Guo M, Li M, Yu X, Wang Y and Wang Y: Hepatocellular carcinoma targeting and pharmacodynamics of paclitaxel nanoliposomes modified by glycyrrhetic acid and ferric tetroxide. *Curr Top Med Chem* 21: 1268-1284, 2021.
55. Cao M, Gao Y, Zhan M, Qiu N, Piao Y, Zhou Z and Shen Y: Glycyrrhizin acid and glycyrrhetic acid modified polyethyleneimine for targeted DNA delivery to hepatocellular carcinoma. *Int J Mol Sci* 20: 5074, 2019.
56. Sang L, Li J, Zhang F, Jia J, Zhang J, Ding P, Sun T and Wang D: Glycyrrhetic acid modified chlorambucil prodrug for hepatocellular carcinoma treatment based on DNA replication and tumor microenvironment. *Colloids Surf B Biointerfaces* 220: 112864, 2022.



Copyright © 2023 Pan *et al.* This work is licensed under a Creative Commons Attribution-NonCommercial-NoDerivatives 4.0 International (CC BY-NC-ND 4.0) License.